19th Australasian Fluid Mechanics Conference
Melbourne, Australia
8-11 December 2014

A Hybrid RANS-Implicit LES Method for External Aerodynamics

A. Islam and B. Thornber

School of Aerospace, Mechanical and Mechatronic Engineering
University of Sydney, New South Wales 2006, Australia

Abstract

Although turbulence-resolving techniques such as Large-eddy Simulation (LES) are quite mature, it still has limited usage for flows at practical Reynolds numbers and this was the main motivation behind the development of detached-eddy simulation (DES) which combines RANS near the wall with LES away from the wall. This paper proposes and compares two novel simulation approaches – the use of a high-order DES and hybrid RANS-Implicit LES (IDES) for a circular cylinder at $Re_D = 3.9 \times 10^3$. Direct comparison is made with results obtained using conventional turbulence models and experimental data in literature. Time-averaged simulation results for the Strouhal number (St) and the mean recirculation length ($\overline{L}_{rec}$) was discussed. The high-order DES results responded well to mesh refinement and produced accurate results for the Strouhal number in the range of 0.209-0.219 but the IDES results had a lower standard-deviation (σ). Stream-wise velocity profiles also agreed well with past experimental data and recirculation regions were captured accurately compared to existing LES results. The results demonstrated the potential of the high-order DES and IDES methods to provide improved performance in capturing and simulating separated flows.

Introduction

Over the last decade, the steady increase in available computational capacity led to the development of more accurate, realistic computational fluid dynamics (CFD) methods for aerodynamics [1]. An understanding of external aerodynamics is also becoming increasingly important for many engineering problems, especially in the automotive industry [2]. It is widely known that a RANS approach often provides insufficient accuracy and transient information for unsteady flows and at relatively high Reynolds numbers encountered in practice ($\sim 10^5 - 10^8$) LES becomes prohibitive especially in the presence of high-Re turbulent boundary layers. A DES approach overcomes this by using a RANS turbulence model in the boundary layers and attached regions of flow transferring to LES in separated regions of flow.

This paper presents a 3D circular cylinder in cross flow which is a generic geometry that has been widely used to evaluate the performance of CFD codes and methods due to some of the interesting flow features which are expected downstream [3, 4, 5, 6]. This includes sensitivity to the Reynolds number regime, which significantly alters the size of the shear layer in addition to the point and mode of separation [3, 4]. The Reynolds number dictates whether turbulent transition occurs on the frontal section of the cylinder, within the boundary layer, or in the detached shear layer. At the subcritical value Re_D=3900, the flow is characterised by a laminar boundary layer and transition to turbulent flow in the detached shear layer [7].

This basic flow domain is also widely used as a test case for basic engineering applications due to its inherent unsteadiness [2]. Although the proposed models are more suitable for fully turbulent flow fields, the current test case is employed to reduce the computational effort. Simulations demonstrate that the flow is essentially laminar aft of the cylinder. Wide availability of LES and experimental results assisted this process of validation [3, 4].

Although the use of first- or second-order numerical schemes is common in engineering, there are some instances where higher-order methods are desirable. Separated flows can benefit greatly from high-order methods. A higher-order method is better able to resolve abrupt gradients and improve the resolution near discontinuities and in unsteady turbulent flows [7]. Previous studies showed that the fifth-order method used here is equivalent to second-order results on eight times the number of grid points.

Both hybrid approaches in this paper are based on a modified, Stability-enhanced Spalart-Allmaras RANS model implemented within the research CFD code FLAMENCO. A Low-Mach number correction scheme had been implemented in the code, to suppress the dependence of the dissipation rate on the Mach number [8]. The existing Implicit LES (ILES) methods implemented in FLAMENCO demonstrated excellent results in the simulation of free-shear layers however, as with conventional LES boundary layers were still expensive to compute [9]. This study explores a simple RANS-ILES coupling which may provide better performance than a standard DES method.

The proposed hybrid turbulence resolving approach seeks to reduce the computational expense required to capture unsteady features for fully separated flow. Primarily this article compares the performances of the new DES and IDES approaches for 3D separated flow over identical geometry to past studies [3, 4].

Computational Approach

Governing Equations

The physics of fluid flow is modelled by the Navier-Stokes equations. They are solved numerically by considering the conservation laws for mass, momentum and energy, in addition to any turbulence models. The algorithm in FLAMENCO utilises a transformation to compute results in curvilinear coordinates (ξ, η, ζ) on multiblock, structured grids –

$$\frac{\partial \mathrm{JU}}{\partial \tau}+\frac{\partial \mathrm{J}\bar{\mathrm{F}}}{\partial \xi}+\frac{\partial \mathrm{J}\bar{\mathrm{G}}}{\partial \eta}+\frac{\partial \mathrm{J}\bar{\mathrm{H}}}{\partial \zeta}=\frac{\partial \mathrm{J}\,\bar{\mathrm{F}}_{\mathrm{v}}}{\partial \xi}+\frac{\partial \mathrm{J}\bar{\mathrm{G}}_{\mathrm{v}}}{\partial \eta}+\frac{\partial \mathrm{J}\bar{\mathrm{H}}_{\mathrm{v}}}{\partial \zeta}+\mathrm{JS} \quad (1)$$

$$\mathrm{J}=\frac{\partial(\mathrm{x},\mathrm{y},\mathrm{z})}{\partial(\xi,\eta,\zeta)} \quad (2)$$

where J is the Jacobian of the coordinate transformation, U is the conserved quantity, F,G,H are inviscid fluxes, the v subscript denotes the viscous fluxes and S is the source term for the underlying Spalart-Allmaras turbulence model equation. A detailed discussion of the FLAMENCO solver can be found in the references cited [7, 8].

Numerical Methods

The FLAMENCO solver relies on non-linear schemes for spatial discretisation and it solves a Riemann problem for the intercell fluxes. The code is a fifth-order spatial and up to third-order temporal compressible solver capable of simulating flows of a Mach number between 10^{-4} to 10 [7, 8]. This combines a Monotone Upstream-Centered Scheme for Conservation Laws (MUSCL) with an approximate HLLC Riemann Solver [11, 12]. Additional details of the solver and the discretisation scheme are available from the respective references cited.

Ultimately a fifth-order accurate scheme was used for the inviscid terms. The Enhanced Stability RANS Spalart-Allmaras model also included modifications to ensure compatibility and stability within this non-linear framework [7, 13]. The Standard Spalart-Allmaras model coefficient $\tilde{\nu}$ was defined as

$$\tilde{\nu}=f_{v1}\Psi\nu \tag{3}$$

$$\text{and } \Psi=\begin{cases}0.05\log\left(1+e^{20\chi}\right) & \chi<10\\ \chi & \chi\geq 10\end{cases} \tag{4}$$

where f_{v1} is a model coefficient and $\chi=\tilde{\nu}/\nu$

This overcame convergence problems at laminar to turbulent interfaces and the negative eddy viscosity values potentially encountered due to boundary cell curvature. Hence this substitution selectively turned off the production, destruction and diffusion terms in the Spalart-Allmaras model $\tilde{\nu}$ equation, resulting in an insensitive advection equation.

For the hybrid DES framework, the performance of the RANS model was retained near the viscous wall boundaries and laminar boundary layers. However, the turbulence eddy destruction equation was affected by the new length scale Δ which replaced the d_w wall distance, similar to traditional DES implementation [5, 14] with C_{DES}=0.65. Hence, outside the boundary layer Δ was based on the cell sizes –

$$\Delta=\min\left(d_w, \Delta_{cell}C_{DES}\right) \tag{5}$$

$$\Delta_{cell}=\sqrt[3]{|J|} \tag{6}$$

Unlike existing studies which used edge sizes, the characteristic size Δ_{cell} is based on the cube-root of the cell Jacobian J (6). This implementation is likely to be more robust with structured grids on curvilinear coordinates.

For the implicit DES approach the effect of the turbulence eddy viscosity on the governing equations were reduced to zero in the free-stream and separated flow regions. Hence, the effective eddy viscosity was defined as –

$$\nu_{eff}=\begin{cases}\nu & \Delta\geq\Delta_{cell}C_{DES}\\ \nu+\nu_t & \Delta<\Delta_{cell}C_{DES}\end{cases} \tag{7}$$

This eliminates modelled turbulent eddy viscosity in the LES regions based on the characteristic length scale Δ. However, in the near-wall regions and boundary layers the enhanced RANS formulation [7] defined previously (4) was maintained. Note that the physical evolution of an eddy is unaffected (7) and this is essential if the flow was to reattach downstream.

Temporal discretisation uses a third-order Strong Stability Preserving Runge-Kutta method (SSPRK) [7, 9]. This achieved additional stabilisation which was needed for the high-order numerical schemes used here. The time-step size was chosen based on the Courant-Fredrichs-Lewy (CFL) condition. The SSPRK method imposed a CFL<3 condition on time-step sizes.

Computational Model

Generally DES requires carefully designed grids which are very case-dependent and require a significant turnaround time [6, 14]. The layout of the domain is shown in Figure 1. The overall domain size was 30D in length, which consisted of 10D upstream and 20D downstream distances, where D is the cylinder diameter (Figure 1), following existing literature [3, 6, 14]. The spanwise length varied significantly in past studies ranging from 2D to 30D. However, a value of 2πD was used here, which is twice the length used by Young [3]. This ensures minimal interference with the boundary conditions and flexibility in cell sizing.

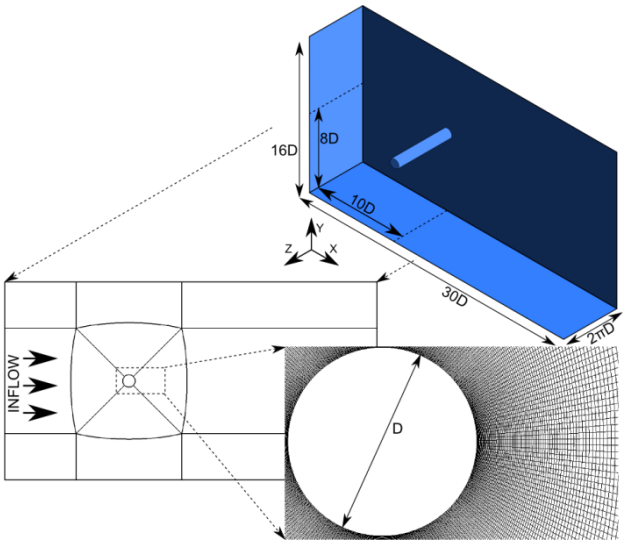

Figure 1. Overall layout and dimensions of the computational domain (top) and near-wall mesh detail on cylinder (bottom).

The domain was initially decomposed into 12 blocks with an O-grid around the cylinder (Table 1a) and a uniform cross-section was maintained for all the simulations. As shown in Table 1, the spanwise mesh consists of 30, 40 and 80 divisions, respectively. Kravchenko and Moin [4] reported that doubling the spanwise size did not significantly affect results if the mesh resolution was maintained, which further justified the fixed span. All meshes had achieved y^+=1.

	N_{total}	y^+	N_θ	N_z	N_{blocks}
(a) Coarse	1,416,708	1	236	30	12
(b) Medium	2,097,360	1	236	40	24
(c) Fine	3,049,600	1	180	80	90

Table 1. Grid parameters flow at Re_D=3900. N represents number of cells. Theta (θ) denotes the circumferential direction and z is the span.

Domain decomposition was efficiently achieved using Open MPI, leading to excellent scalability for FLAMENCO. All grids in Table 1, were multiblock, structured and generated in a CGNS format for greater flexibility and its wide compatibility within the research CFD community.

The flow field was initialised using a Reynolds number, Mach number and a constant fluid viscosity. The Reynolds number was 3.9×10^3 for all simulations. A Mach number of 0.2 was used here. Although this was a source of error for the local density which would vary by up to 2% due to compressibility, it was justified due to the larger time-step and faster turnaround.

Initially all cases used the Stability-enhanced Spalart-Allmaras RANS model [7] for the first 10 vortex shedding cycles. The characteristic length scale modifications were then turned on, for a DES simulation over a period of 20-30 shedding cycles. This was further used to initialise the implicit DES cases.

A subsonic inlet was defined at 10D upstream of the cylinder with a corresponding subsonic outlet at 20D downstream of the cylinder (Figure 1). The top and the bottom boundaries were inviscid walls placed at 8D distances above and below the cylinder. This impermeable boundary led to a zero-shear condition for the fluid at the interface. The 1 m diameter (D) cylinder surface was defined as a viscous wall boundary and this

was placed at the origin of the coordinate system. A planar symmetry condition was used for the left and right boundaries.

Ultimately, CFL=1.5 was used for all simulations. These simulations spanned a period of 2000 seconds of physical flow time and transient statistics were collected over the last 10 shedding cycles. Results for time-averaging were sampled at every 5 second intervals, or 10 per shedding cycle. This is a larger period than Kravchenko and Moin ($T=35D/U_0$) [4].

Results

In order to assess the performance of the two different models proposed in this study, results are compared against both computational and experimental data. The Strouhal number was calculated using the unsteady lift and drag results collected over at least 10 shedding cycles. A Fast Fourier Transform (FFT) was used for each of the datasets and the dominant frequencies were used to calculate $St=fD/\bar{u}$.

The prediction of the mean recirculation length ($\bar{L}_{rec}/D$) in the flow field aft of the cylinder was also included. This is important since the mean velocity profiles depend on the shedding frequency it also has an impact on the mean size of the wake and hence, the overall pressure drag induced by the cylinder.

	St	$\bar{L}_{rec}/D$
Enhanced S-A DES Coarse	0.219	1.08
Enhanced S-A DES Medium	0.217	1.92
Enhanced S-A DES Fine	0.209	1.51
Implicit DES Coarse	0.216	0.99
Implicit DES Medium	0.212	1.35
Implicit DES Fine	0.219	1.53
Experimental [15]	--	1.66
Experimental [3, 16, 17]	0.215±0.005	1.4±0.1
LES [4]	0.210	1.35

Table 2. Summary of the overall flow parameters obtained for at least 10 shedding cycles. Table 1 defined the various mesh refinement levels.

From Table 2 it can be observed that the majority of the simulations presented lie within the accepted range defined by past experimental studies at this Reynolds number range. All the Enhanced Spalart-Allmaras DES simulations showed a gradual reduction in the Strouhal number with increased mesh refinement. The finest mesh DES Strouhal number prediction only varied 0.4% from both the referenced LES result and the lower bound for the experimental data. The Implicit DES did not demonstrate this trend for either the Strouhal number or the recirculation lengths. The Implicit DES approach produced good results for all refinement levels however, the medium mesh having ~2.06 million cells was found to be optimal. The Strouhal number and recirculation lengths were within 1.3% and 3.5% of experimental observations [3].

The stream-wise velocity profiles downstream of the cylinder are shown in Figure 2 and 3 provided additional information about flow features such as the roll up of the shear layer. Figure 2 shows the recirculation length as the zero stream-wise velocity and as expected, the finest mesh was the most accurate immediately after separation (x/D<3).

The referenced coarse-medium mesh LES results [3] were similar to the medium mesh results in the near-wake region which might be an indication of the DES and Implicit DES approaches both rapidly switching out of RANS mode.

The finest mesh results show different behaviour corresponding to the DES and Implicit DES approaches, with an over-prediction and under-prediction of the peak velocity deficit, respectively. However, it is important to note that the recirculation lengths were accurate to 7.8% of experiments [15] and IDES was more successful in predicting the location of the peak.

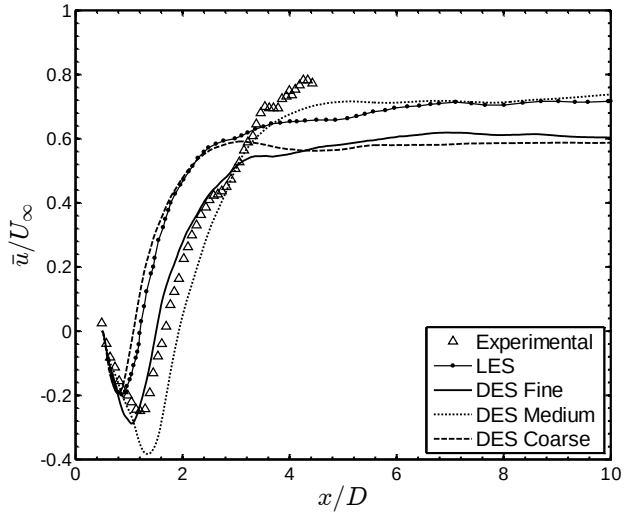

Figure 2. Stream-wise non-dimensionalised velocity on the centre line in the wake of the cylinder using DES approach. Results have been truncated to x/D=10 and the LES results used 1.44×10^6 cells [3] LES and Experimental results were from Lourenco and Shih [15].

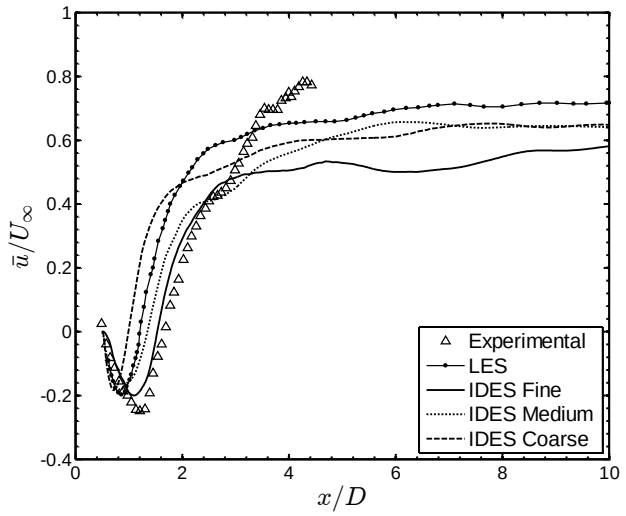

Figure 3. Stream-wise non-dimensionalised velocity on the centre line in the wake of the cylinder using the IDES approach. Results have been truncated to x/D=10 and the LES results used 1.44×10^6 cells [3] LES and Experimental results were from Lourenco and Shih [15].

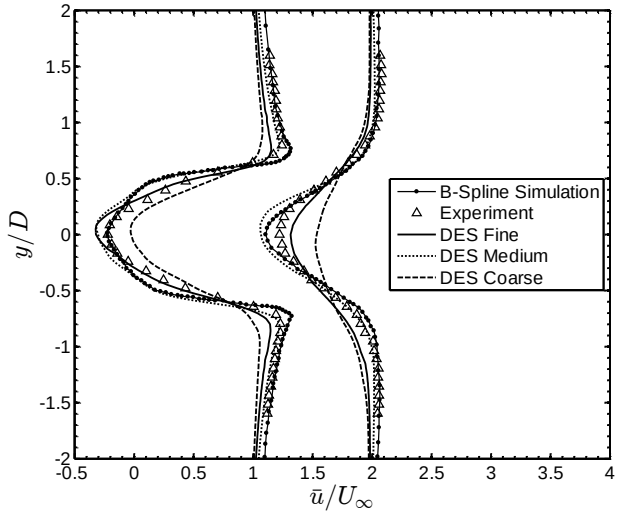

Figure 4. Stream-wise velocity profiles in the wake of the cylinder with a DES approach taken at x/D=1.06 (left) and 2.02 (right). B-Spline simulation – [4] and Experimental results – [15].

The velocity profiles reveal that both the DES and IDES resolved the peak deficits at x/D=1.06 and were within 7% of experimental data as shown in Figure 4 and 5.

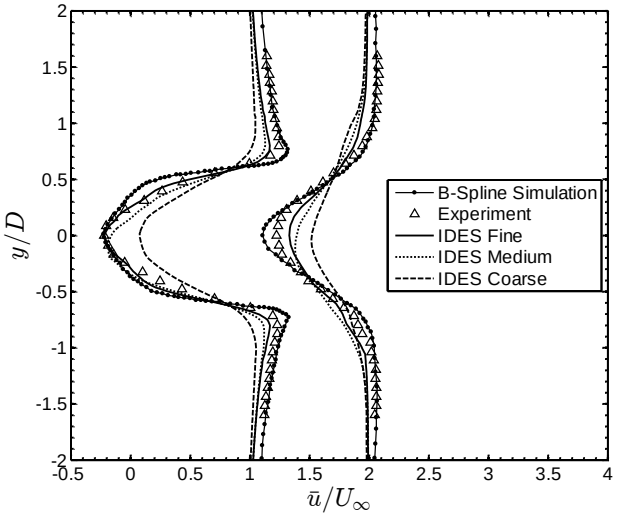

Figure 5. Stream-wise velocity on the centre line in the wake of the cylinder an IDES approach taken at x/D=1.06 (left) and 2.02 (right). B-Spline simulation – [4] and Experimental results – [15].

The recovery and shear layer dissipation (x/D=2.02) was better predicted by the B-Spline simulation however, this might be an artefact of the flow being accelerated, as seen by the overshoot in the shear layer roll up and free-stream velocity profiles.

Conclusion

This article proposed two different hybrid turbulence modelling approaches and presented a preliminary assessment of their performance in a sub-critical Reynolds number flow with relatively large separation. The Enhanced Spalart-Allmaras-based DES model utilised a modified definition of the characteristic length scale and Implicit DES, removes the modelled turbulent eddy viscosity from the momentum equations.

Overall, both the DES and IDES approaches captured the near-wake recirculation profiles immediately aft of the cylinder. There was a larger difference observed in the free-stream between the referenced LES results, experimental data and the models presented here. The location of the peak velocity deficit in the IDES recirculation profiles improved relative to experimental data, with successive mesh refinement. Both methods were able to capture the separated shear layer in the wake of the cylinder inspected at two locations.

This paper also showed significant potential for improvements of the algorithm and a blending function for IDES is currently in development. Additionally note that the implicit DES method here is likely to achieve improved prediction of fully turbulent flow phenomena however, this preliminary case at Re_D=3900 still led to good agreement with both past studies.

References

[1] Sagaut, P. & Deck, S., Large eddy simulation for aerodynamics: status and perspectives, *Philosophical Transactions of the Royal Society of London*, **367**, 2009, 2849-2860.

[2] Islam, M., Decker, F., de Villiers, E., Jackson, A., Gines, J., Grahs, T., Gitt-Gehrke, A., & Comas i Font, J., Application of Detached-Eddy Simulation for Automotive Aerodynamics Development, *Society of Automotive Engineers, Technical Report SAE 2009-01-0333*, 2009.

[3] Young, M. E & Ooi, A., Comparative Assessment of LES and URANS for Flow over a cylinder at a Reynolds number of 3900, in *Proceedings of the 16th Australasian Fluid Mechanics Conference*, 2007, 1063-1070.

[4] Kravchenko, A.G. & Moin, P., Numerical Studies of flow over a circular cylinder Re_D=3900", *Physics of Fluids*, **12**, no. 2, 2000, 403-417.

[5] Spalart, P. R., Deck, S., Shur, M. L., & Squires, K. D., A new version of detached-eddy simulation, resistant to ambiguous grid densities, *Theoretical and Computational Fluid Dynamics*, **20**, no. 3, 2006, 181-195.

[6] Travin, A., Shur, M., Strelets, M. & Spalart, P., Detached-Eddy Simulations Past a Circular Cylinder, *Flow, Turbulence and Combustion*, **63**, 1999, 293-313.

[7] Juarez, A.G., Raimo, A., Shapiro, E. & Thornber, B., Steady Turbulent Flow Computations Using a Low Mach Fully Compressible Scheme, AIAA Journal, Preprint – AIAA Early Edition, 2014, 1-17, DOI: 10.2514/1.J052948

[8] Thornber, B., Mosedale, A., Drikakis, D. & Williams, R. J. R., An improved reconstruction method for compressible flows with low Mach number features, *Journal of Computational Physics*, **227**, 2008, 4873-4894.

[9] Drikakis, D., Hahn, M., Mosedale, A. & Thornber, B., Large eddy Simulation using high-resolution and high-order methods, *Philosophical Transactions of the Royal Society of London*, **367**, 2009, 2985-2997.

[10] Thornber, B. & Drikakis, D., Numerical dissipation of upwind schemes in low Mach flow, *International Journal for Numerical Methods in Fluids*, **56**, no. 8, 2007, 1535-1541.

[11] Harten, A., Lax, A. & van Leer, B., On Upstream Differencing and Godunov-Type Schemes for Hyperbolic Conservation Laws, *SIAM Review*, **25**, no. 1, 1983, 35-61.

[12] Toro, E., Spruce, M. & Speares, W., Restoration of the Contact Surface in the HLL-Riemann Solver, *Shock Waves*, **4**, no. 1, 1994, 25-34.

[13] Burgess, N.K., Mavriplis, D., Robust Computation of Turbulent Flows using a Discontinuous Galerkin Method, in *50th AIAA Aerospace Sciences Meeting and Exhibit*, 2012.

[14] Squires, K.D., Krishnan, V., & Forsythe, J.R., Prediction of the flow over a circular cylinder at high Reynolds number using detached-eddy simulation," *Journal of Wind Engineering and Industrial Aerodynamics*, **96**, 2008, 1528-1536.

[15] Lourenco, L.M., & Shih, C., Characteristics of the plane turbulent near wake of a circular cylinder. A particle image velocimetry study, reported in [4]

[16] Breuer, M., Large eddy simulation of the subcritical flow past a circular cylinder: numerical and modelling aspects, *International Journal of Numerical Methods in Fluids*, **28**,1998, 1281-1302, reported in [3].

[17] Norberg, C., Fluctuating lift on a circular cylinder: review and new measurements, *Journal of Fluids and Structures*, **17**, 2003, 57-96, reported in [3].